Stability and sensitivity analysis of the secondary instability in the sphere wake

Vincenzo Citro, Lorenzo Siconolfi, David Fabre, Flavio Giannetti, Paolo Luchini

Stability and Sensitivity Analysis of the Secondary Instability in the Sphere Wake

Vincenzo Citro*
Universitá degli Studi di Salerno, 84084 Fisciano (Salerno), Italy
Lorenzo Siconolfi†
Universitá di Pisa, 56122 Pisa, Italy
David Fabre‡
Université de Toulouse, F-31400 Toulouse, France
and
Flavio Giannetti§ and Paolo Luchini§
Universitá degli Studi di Salerno, 84084 Fisciano (Salerno), Italy

The three-dimensional flow past a fixed sphere placed within a uniform stream is investigated. This paper focuses on the second bifurcation, which is responsible for the onset of the unsteadiness. Using the highly efficient Nek5000 parallel solver together with a recently developed numerical algorithm to stabilize and accelerate the numerical solution, it was possible to identify the three-dimensional eigenmode responsible for the second bifurcation. The characteristics of this eigenmode are analyzed in detail. The value of the critical Reynolds number $Re_{cr}^{II} = 271.8$, as well as the Strouhal number of the arising limit cycle, agree well with previous experimental and numerical investigations. To further assess the nature of the instability, an adjoint-based sensitivity analysis is carried out. The structure of the direct and adjoint modes are discussed, and then the core of the instability is localized. Finally, the sensitivity of the instability to a generic base flow modification is investigated.

I. Introduction

THE flow past a three dimensional bluff body is an important topic of research due to its relevance in industrial processes. Dedicated literature on such flows indicates that wakes produced by cylinders can display different behaviors compared with those produced by a three dimensional bluff body like a sphere. The earliest documented experimental activity was performed by Taneda [1], where the flow past a sting mounted sphere for Reynolds numbers, based on the diameter of the sphere and the incoming uniform velocity, ranging from 5 to 300 was investigated using flow visualization techniques. He showed that a recirculating region develops close to the rear stagnation point at about $Re \approx 24$ and it expands up to $Re \approx 130$. Above this value, he observed a first instability of the flow characterized by periodic oscillations of the wake with a long time period. Achenbach [2] and Sakamoto and Haniu [3], using the same experimental setup, documented the characteristics of the sphere wake considering Reynolds numbers up to 10^5. However, some discrepancies among the results from these experimental investigations were found due to the different experimental setups. In particular, Ormières [4] demonstrated that the experimental measurements have a significant sensitivity from the perturbations introduced by the supports of the sphere. Despite this difficulty, the transition scenario in the range $150 < Re < 350$ is widely accepted. Table 1 summarizes the estimated critical Reynolds numbers for the first Re_{cr}^{I} and second Re_{cr}^{II} bifurcation found in the dedicated literature [3,5 11]. Magarvey and Bishop [5] used dye visualization to study the wakes of free falling drops of an immiscible liquid in water and showed in detail the characteristics of the different transitions. Natarajan and Acrivos [6] reported the presence of a steady axisymmetric flow solution up to $Re = 210$, where another steady state occurred, but characterized by an asymmetric flow field. As Reynolds number is increased, the flow pattern changes again at $Re \approx 280 \pm 10$. Above this threshold, an unsteady flow state is observed. Several flow visualizations of the steady asymmetric regime (see, e.g., Johnson and Patel [7]) confirm that the axial symmetry of the flow field at low Reynolds number is replaced by a planar symmetry, which is also preserved above the second bifurcation.

For a long time, numerical computations of the flow behind a sphere have been confined to axisymmetric configurations due to the large computational costs involved in a fully three dimensional simulation. Tomboulides et al. [8] were the first to perform accurate three dimensional (3 D) direct numerical simulations (DNSs) by using spectral methods. They provided the critical Reynolds number for the loss of the axial symmetry at $Re_{cr}^{I} = 212$. Moreover, they also observed the onset of unsteadiness between $Re = 250$ and $Re = 285$. Natarajan and Acrivos [6] examined the linear instability of the steady axisymmetric base flow to three dimensional modal perturbations. They reported the occurrence of a supercritical bifurcation, at a critical Reynolds number of $Re \approx 210$, characterized by unitary azimuthal wavenumber. Subsequently, the numerical study by Ghidersa and Dušek [9] allowed one to obtain a more accurate characterization of the first and second bifurcation, combining a Fourier expansion in azimuthal direction with a spectral element discretization analogous to [8]. In particular, they identified a breaking of axisymmetry at $Re_{cr}^{I} = 212$ and the onset of the unsteadiness at $Re_{cr}^{II} = 272.3$. In addition, using the same numerical scheme, Bouchet et al. [10] have shown that the instabilities for the flow past a sphere leads to the onset of a lift and also of a torque, which become oscillating quantities when the secondary instability is reached. Moreover, Pier [12] performed a local stability analysis on the planar symmetric base flow, under the assumption of weakly nonparallel flow, to predict the occurrence of the second bifurcation. Unfortunately, as for the cylinder case, the nonparallel effects of the wake region negatively affects the accuracy of the results. Fabre et al. [13] introduced a model based on the theory of mode interactions in the presence of $\mathcal{O}(2)$ symmetry: They were able to build a consistent bifurcation diagram. However, their assumption of simultaneous

*DIIN, Via Giovanni Paolo II; vcitro@unisa.it.
†DICI, Via Girolamo Caruso.
‡INPT, UPS, IMFT Alle´e Camille Soula.
§DIIN, Via Giovanni Paolo II.

Table 1 Summary of main results documented in literature for the transition scenario of flow past a sphere[a]

Source	Type	Re_{cr}^{I}	Re_{cr}^{II}	St^{II}	St^{Re^*}
Magarvey and Bishop [5]	Exp	210	280 ± 10		≈ 0.10
Sakamoto and Haniu [3]	Exp		300		≈ 0.14
Natarajan and Acrivos [6]	Num	210	277.5		0.137
Tomboulides et al. [8]	Num	212	250/285		0.136
Johnson and Patel [7]	Num	211	270/280		0.137
Ghidersa and Dušek [9]	Num	212	272.3	0.127	
Bouchet et al. [10]	Num	211.9	274	0.128	0.136
Szaltys et al. [11]	Exp	212	268	0.18	

[a]In particular, we report the critical Reynolds number for the first Re_{cr}^{I} and second bifurcation Re_{cr}^{II} and the Strouhal number at $Re = Re_{cr}^{II}$ and $Re = Re^* = 300$ (Exp = experimental, Num = numerical).

nearly neutral modes is closely satisfied for the flow past a thin disk, but not for the sphere. In this last case, the model does not accurately predict the critical Reynolds number for the first and the second bifurcation.

In this context, we perform a full three dimensional global stability analysis to accurately determine the occurrence of the second bifurcation. To characterize the physical mechanism giving rise to the instability, we compute the adjoint global mode and perform a structural sensitivity analysis as introduced by Giannetti and Luchini [14]. Finally, the sensitivity of the complex eigenvalue to a generic base flow modification is presented.

II. Problem Formulation

A. Flow Configuration and Governing Equations

In this paper, we consider the uniform flow of an incompressible fluid over a solid sphere. The flow field is described using a Cartesian coordinate system whose origin coincides with the center of the sphere and with the x axis aligned with the incoming flow direction (see Fig. 1a).

The fluid motion is described by the three dimensional unsteady incompressible Navier Stokes equations:

$$\nabla \cdot \boldsymbol{u} = 0 \tag{1a}$$

$$\frac{\partial \boldsymbol{u}}{\partial t} + \boldsymbol{u} \cdot \nabla \boldsymbol{u} = -\nabla P + \frac{1}{Re} \nabla^2 \boldsymbol{u} \tag{1b}$$

where $\boldsymbol{u} = [u, v, w](\boldsymbol{x}, t)$ is the velocity vector and $P(\boldsymbol{x}, t)$ is the reduced pressure. The system of partial differential equations (1) is made dimensionless using the sphere diameter D as the characteristic length scale and the freestream velocity U_∞ as the reference velocity. The Reynolds number of the problem is $Re = U_\infty D/\nu$ where ν is the kinematic viscosity of the fluid. Equations (1) are completed with appropriate boundary conditions. In particular, on the sphere surface Ω_s, no slip and no penetration conditions are enforced, whereas a uniform velocity distribution is considered at the inlet boundary Ω_{in} ($\boldsymbol{u} = [U_\infty, 0, 0]$). Symmetry conditions are imposed on the lateral Ω_{lat} boundaries, whereas outflow conditions (stress free or natural conditions in a finite element context) are used at the outlet Ω_{out}.

B. Global Stability and Sensitivity Approach

The occurrence of a self excited (global) mode is studied here in the framework of a linear analysis by using a normal mode decomposition. The total flow field $[\boldsymbol{u}, P](\boldsymbol{x}, t)$ is decomposed into a steady flow solution $[\boldsymbol{U}_b, P_b](\boldsymbol{x})$, usually referred as *base flow*, and a small unsteady perturbation $[\boldsymbol{u}', P'](\boldsymbol{x}, t)$ as

$$\boldsymbol{u}(x, y, z, t) = \boldsymbol{U}_b(x, y, z) + \varepsilon \boldsymbol{u}'(x, y, z, t) \tag{2a}$$

$$P(x, y, z, t) = P_b(x, y, z) + \varepsilon p'(x, y, z, t) \tag{2b}$$

where ε is assumed small. Introducing Eq. (2) into Eq. (1) and linearizing, we obtain two problems describing the spatial structure of the base flow and the evolution of the unsteady perturbation. In particular, the disturbance is governed by the linearized Navier Stokes equations:

$$\nabla \cdot \boldsymbol{u}' = 0 \tag{3a}$$

$$\frac{\partial \boldsymbol{u}'}{\partial t} + \boldsymbol{U}_b \cdot \nabla \boldsymbol{u}' + \boldsymbol{u}' \cdot \nabla \boldsymbol{U}_b = -\nabla P' + \frac{1}{Re} \nabla^2 \boldsymbol{u}' \tag{3b}$$

To investigate the long term (asymptotic) stability, the evolution of the perturbation is expressed by means of the classical normal mode form:

$$[\boldsymbol{u}', P'](x, t) = \sum_n [\hat{\boldsymbol{u}}_n, \hat{P}_n](x) \exp\{(\sigma_n + i\omega_n)t\} + \text{c.c.} \tag{4}$$

where c.c. designates the complex conjugate terms.

Thus, the disturbance behavior is described by the complex eigenvector $[\hat{\boldsymbol{u}}_n, \hat{P}_n]$ and the complex eigenvalue $\lambda_n = \sigma_n + i\omega_n$, where ω_n is the eigenfrequency and σ_n represents the growth rate. By introducing such ansatz (4) into the linearized Navier Stokes equations (3), we are left with an eigenvalue problem

$$\nabla \cdot \hat{\boldsymbol{u}}_n = 0 \tag{5a}$$

$$\{\sigma_n + i\omega_n\}\hat{\boldsymbol{u}}_n + \boldsymbol{U}_b \cdot \nabla \hat{\boldsymbol{u}}_n + \hat{\boldsymbol{u}}_n \cdot \nabla \boldsymbol{U}_b = -\nabla \hat{P}_n + \frac{1}{Re} \nabla^2 \hat{\boldsymbol{u}}_n \tag{5b}$$

These equations are supplemented with appropriate boundary conditions. In particular, we impose $\hat{\boldsymbol{u}}_n = 0$ on the sphere wall Ω_s and at the inlet section Ω_{in}, whereas on the rest of the boundaries, we use the same conditions as used for the base flow calculations. Ordering the eigenvalues by their growth rates in descending order ($\sigma_0 \geq \sigma_1 \geq \sigma_2 \geq, \cdots$), the asymptotic stability of the flow is driven by the leading global eigenpair $(\sigma_0 + i\omega_0; \hat{u}_0, \hat{P}_0)$. In particular, the system is stable if the growth rate of the leading eigenvalue is negative ($\sigma_0 < 0$), whereas it is unstable if the growth rate is positive ($\sigma_0 > 0$).

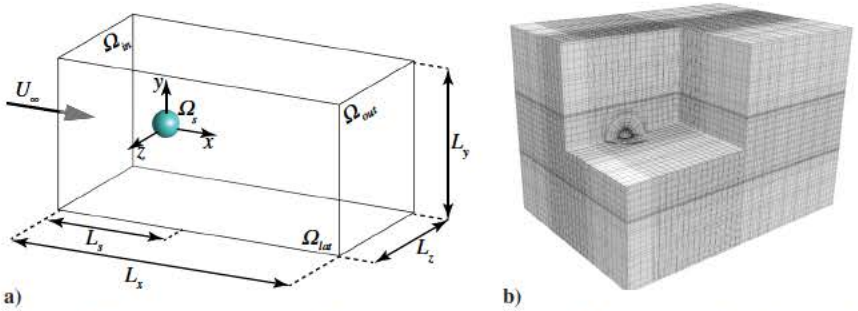

Fig. 1 Representation of a) flow configuration and frame of reference; b) typical mesh used for computations. For a complete and detailed list of the parameters and grids used, see Table 2.

To localize the core of the instability (i.e., the region where the instability mechanism acts on the base flow), the structural sensitivity analysis introduced by Giannetti and Luchini [14] is carried out. This analysis allows one to quantify the effect of a small localized perturbation $\delta\mathcal{L}$ of the structure of the linear operator $\delta\mathcal{L}(\boldsymbol{U}_b, \hat{\boldsymbol{u}}; Re) = \boldsymbol{U}_b \cdot \nabla\hat{\boldsymbol{u}} + \hat{\boldsymbol{u}} \cdot \nabla\boldsymbol{U}_b - Re^{-1}\nabla^2\hat{\boldsymbol{u}}$ on the eigenvalue λ. Introducing the adjoint operator $\mathcal{L}^\dagger$ (see Luchini and Bottaro [15] for a complete review on the role of the adjoint), the instability core can be determined by introducing the sensitivity tensor $\boldsymbol{S}$, that can be defined as

$$\boldsymbol{S}(x, y, z) = \frac{\hat{\boldsymbol{u}}^\dagger \otimes \hat{\boldsymbol{u}}}{\langle \hat{\boldsymbol{u}}^\dagger | \hat{\boldsymbol{u}} \rangle} \tag{6}$$

Here, the inner product $\langle \cdot | \cdot \rangle$ between two complex vectors is defined as follows:

$$\langle \boldsymbol{a} | \boldsymbol{b} \rangle \int_\Omega \boldsymbol{a}^* \cdot \boldsymbol{b} \, \mathrm{d}\Omega \tag{7}$$

where the superscript $*$ denotes the conjugate of the complex quantity and Ω is the computational domain. Thus, following Giannetti and Luchini [14], we localize the instability core by first evaluating the spatial sensitivity map $S(x, y, z) = \|S(x, y, z)\|_2$ and then inspecting the region where it attains the larger values. It has been also shown that this region is similar to that in which it is necessary to introduce a small cylinder to control the dynamics of the wake [14].

However, the introduction of a small control cylinder in a bluff body wake also modifies the base flow and thus alters the stability properties of the flow. To take into account this latter aspect, the concept of sensitivity analysis to base flow modifications has been introduced first by Bottaro et al. [16] and then by Marquet et al. [17]. This procedure allows one to define the variation of the eigenvalue $\delta\lambda$ produced by a generic small amplitude modification of the base flow $\delta\boldsymbol{U}_b$, evaluated as

$$\delta\lambda = \frac{\langle \boldsymbol{S}_b | \delta\boldsymbol{U}_b \rangle}{\langle \hat{\boldsymbol{u}}^\dagger | \hat{\boldsymbol{u}} \rangle} \quad \text{with } \boldsymbol{S}_b(x, y, z) = -(\nabla\hat{\boldsymbol{u}})^H \cdot \hat{\boldsymbol{u}}^\dagger + \nabla\hat{\boldsymbol{u}}^\dagger \cdot \hat{\boldsymbol{u}}^* \tag{8}$$

where H denotes the Hermitian matrix. Thus, the sensitivity $\boldsymbol{S}_b(x, y, z)$ is a complex vector field, where the real part $\boldsymbol{S}_{b,r}$ and the imaginary part $\boldsymbol{S}_{b,i}$ are the sensitivities of the growth factor and of the frequency to a generic base flow modification, respectively.

III. Direct Numerical Simulation and Linear Time Stepper for Global Instability Computations

The nonlinear DNSs are performed using the code NEK5000. It adopts the spectral element method to discretize the governing equations. We chose this code for its accuracy, efficiency, and flexibility in treating complex geometries. For further details, we refer to Patera [18] and Fischer [19]. Here, we adopt the classical $P_N - P_{N-2}$ formulation using a discretization that involves Lagrange orthogonal polynomials on the Gauss Lobatto Legendre nodes.

When investigating the problem under the framework of linear stability analysis, the first step consists of computing a steady three dimensional base flow. As one requires to compute such a base flow both below and above the stability threshold (where it is unstable), one cannot simply use standard time integration of the Navier Stokes equations up to convergence, and a specific numerical method is required.

In the present work, the base flows are computed using our in house stabilization algorithm called BoostConv (see Citro et al. [20] Appendix A). The leading linear direct and adjoint modes are then computed using the ParPACK implementation of the Implicitly Restarted Arnoldi Method, which has been coupled to the direct linear and adjoint time steppers available in Nek5000 (see Tammisola et al. [21] and Lashgari et al. [22] for further details).

For both DNS and global stability analyses, we have used four different meshes consisting of multiblock grids, for which the characteristics are given in Table 2. A representative sectional view of the mesh M4 is shown in Fig. 1b. Note that the meshes are symmetric with respect to both plane $z = 0$ and $y = 0$ and are refined in the vicinity of the surface of the sphere to correctly resolve the boundary layers. To validate our method, we performed several numerical tests to study the effects of the resolution and of the size of computational domain on the flow stability. A grid convergence analysis was performed to select the best grid in terms of speed and accuracy. We found that the leading eigenvalues vary less than 0.05% when the number of elements and the polynomial order N_p are increased and the inlet or the outlet regions are moved apart. The results of such tests are reported in Tables 2 and 3.

Table 2 Meshes used in the present study to validate the numerical setup[a]

Mesh	L_x	L_y	L_z	L_s	N_p	$N_{\text{elem.}}$
M1	40	20	20	10	10	8,510
M2	47	24	24	12	10	12,920
M3	47	24	24	12	13	12,920
M4	52	28	28	14	13	15,160

[a]N_p is the degree of the polynomial used in Nek5000 and $N_{\text{elem.}}$ is the total number of elements; see Fig. 1 for the nomenclature.

Table 3 Influence of spatial grid resolution and domain extension on the critical Reynolds numbers $Re_{\text{cr}}^{\text{I}}$ and $Re_{\text{cr}}^{\text{II}}$

Mesh	$Re_{\text{cr}}^{\text{I}}$	$Re_{\text{cr}}^{\text{II}}$
M1	212.8	272.9
M2	212.5	272.1
M3	212.4	271.9
M4	212.4	271.8

As presented in Table 2, it is possible to perform a p refinement, increasing the polynomial order of the spectral elements, or an h refinement by increasing the total number of elements inside the computational domain. Tables 3 and 4 show that the length of the computational domain does not influence the leading eigenvalues, whereas the polynomial order weakly affects the results. It should be noted that the size of the computational domain generally affects the numerical results. However, as discussed in [14], we emphasize here that, to accurately compute the eigenvalue of interest, it is sufficient to have enough resolution in the corresponding "wavemaker" region.

Table 4 Strouhal number computed by using DNS and linear global 3-D stability analysis at $Re = 275$[a]

Mesh	St_{Stab}	St_{DNS}
M1	0.128	0.1296
M2	0.129	0.1303
M3	0.129	0.1306
M4	0.129	0.1307

[a]The present Strouhal number computed by using DNS is extracted using a probe measuring the velocity norm at $(3.5D, 0.1D, 0.1D)$.

IV. Results

A. Direct Numerical Simulations

The wake flow past a fixed sphere has been initially characterized by using DNSs. For Reynolds numbers smaller than $Re_{\text{cr}}^{\text{I}} = 212.4$, the base flow is axisymmetric with the same spatial structure in every plane that passes through the x axis. The flow topology consists of a toroidal recirculation region with closed streamlines. As the Reynolds number is increased beyond the threshold value $Re_{\text{cr}}^{\text{I}}$, the system loses its axial symmetry and a new asymmetric base flow with a planar symmetry

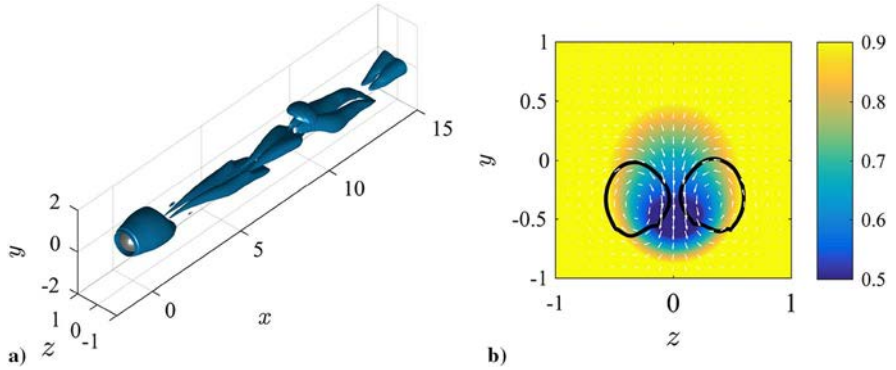

Fig. 2 Representative a) isosurface of the λ_2 criterion for the unsteady flow field solution at $Re = 280$; b) cross section at $x = 5D$. Color contours show the x velocity, white arrows show the in-plane velocity, and black thick lines are representative contour of the vortical structure highlighted by the λ_2 criterion.

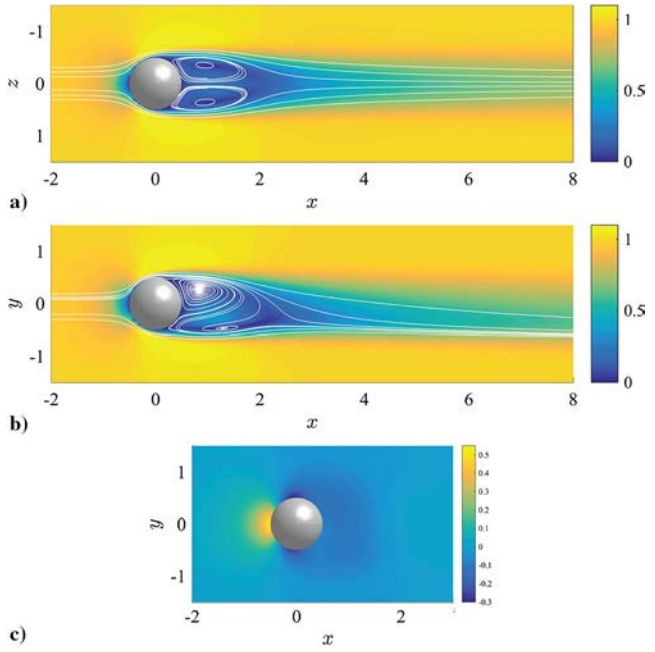

Fig. 3 Stabilized supercritical base flow around a sphere for $Re = 275$: a) top and b) front view of the velocity magnitude in the median planes (white solid lines are representative in-plane streamlines); c) front view of the pressure field for a section at $z = 0$.

emerges. The critical Reynolds number obtained for the first bifurcation is in good agreement with the results obtained using a $2.5D$ analysis by Meliga et al. [23]. However, we are here mainly interested in the onset of the unsteadiness (i.e., in determining the occurrence of the second bifurcation). Direct numerical simulations of the full 3 D Navier Stokes equations are used to perform a parametric analysis of the wake flow past the sphere at larger Reynolds number. Results show that, for $Re > Re_{\mathrm{cr}}^{\mathrm{II}} = 271.8$, the flow becomes unsteady. A typical snapshot of the unsteady flow field at $Re = 280$ is depicted in Fig. 2.

Figure 3 shows the spatial distribution of the base flow for the unstable steady state at $Re = 275$. In particular, Fig. 3a depicts the isocontours of the velocity modulus in the x z plane (see Fig. 1 for the frame of reference), together with representative streamlines. In this top view, we can clearly observe that the flow is symmetric. Figure 3b shows the velocity distribution in the inherent symmetry plane x y. The streamlines in the symmetry plane are no longer closed, but are spiraling toward a converging focus in the upper half and outward from a diverging focus in the lower half. Johnson and Patel [7] described this flow feature: It indicates a three dimensional flow along the toroidal structure, with streamlines diverging in the third direction from the upper focus and converging toward the lower one. The pressure distribution is also depicted in Fig. 3c. The arising asymmetric pressure field causes a net lift force acting on the sphere [24].

Figure 4a shows the evolution of the Strouhal number $St_{\mathrm{DNS}} = f_{\mathrm{DNS}} D/U_\infty$ predicted by DNS as a function of the Reynolds number, f_{DNS} being the frequency of the limit cycle evaluated from a probe measuring the velocity norm in the flow field located at $(3.5D, 0.1D, 0.1D)$. Our results are in good agreement with [10].

Finally, the saturated amplitude of the lift coefficient $C_L = F_y/[(\rho U_\infty^2/2)(\pi D^2/4)]$ as a function of the Reynolds number is evaluated from the DNS results and it is reported in Fig. 4b. Here, we can easily confirm the presence of a square root scaling such behavior ($C_L \propto \sqrt{Re - Re_{\mathrm{cr}}}$), which is a typical footprint of a supercritical Hopf bifurcation, as already discussed in [10]. By using a polynomial (quadratic) fitting of this DNS data and extrapolation, we estimate a critical Reynolds number of $Re \approx 273$.

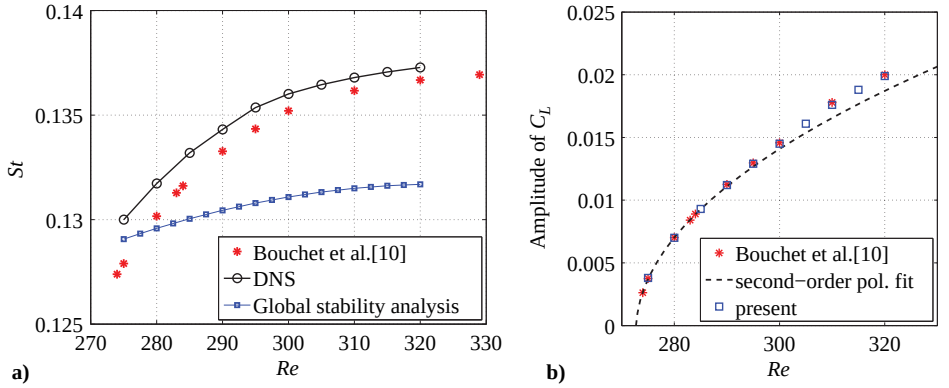

Fig. 4 Graph of a) Strouhal number as a function of Reynolds number: Comparison between DNS data and global stability results; b) saturation amplitude of the oscillating part of the lift coefficient measured as a function of Reynolds number. Dashed line represents the second-order polynomial fit (pol. fit) to the DNS data. The $*$ symbols are adopted to report the results discussed in [10].

B. Stability and Sensitivity Analysis

To confirm that the occurrence of the onset of unsteadiness is effectively due to a Hopf bifurcation, we apply a full three dimensional stability analysis on top of the stabilized steady base flow. As explained in Sec. II.B, this approach allows one to compute the eigenvalue of the leading mode under the form $\sigma_0 + i\omega_0$. The inspection of the growth rate σ_0 allows prediction of the threshold of the second bifurcation. As discussed in Sec. III, we used different meshes to perform a grid convergence study. Results reported in Table 3 clearly indicate a threshold at $Re_{\mathrm{cr}}^{\mathrm{II}} = 271.8$.

Because the dynamics of the flow is driven by the leading unstable eigenmode, the imaginary part of the eigenvalue ω_0 provides an estimation of the Strouhal number $St_{\mathrm{Stab}} = \omega_0 D/2\pi U_\infty$ of the limit cycle arising from the bifurcation. This quantity is plotted in Fig. 4a, together with the Strouhal number effectively observed in the DNS and those from the literature (see, for instance, [25]). The results show that the global stability analysis is able to predict the DNS Strouhal number only near the $Re_{\mathrm{cr}}^{\mathrm{II}}$: Nonlinear interactions and saturation become rapidly important, increasing the Reynolds number.

Figures 5a 5c show the spatial distribution of the leading direct global mode by using representative isosurfaces of the three velocity components. We can note that the structure of this global mode is dominated by streamwise velocity fluctuations located downstream of the bluff body. As shown in Fig. 3, the base flow is plane symmetric with respect to the x y plane. The streamwise u and transverse v velocity components of the global mode have the same planar symmetry: They are symmetric with respect to the x y plane. The spanwise w velocity component is antisymmetric with respect to such plane. From a physical point of view, the resulting unsteady flow (which derives from the superposition of the base flow and the perturbation) preserves the planar symmetry. This finding is in agreement with the results reported by Tomboulides and Orszag [25].

The adjoint mode is depicted in Fig. 6. The spatial structure of this field is localized near the sphere surface with the maximum peak attained in the lower part of the near wake. The adjoint mode has the same planar symmetry as the direct mode. We recall that the adjoint can be used to study the receptivity of the mode to a generic initial condition or forcing term. In particular, if the forcing function (added to the right hand side of the momentum equation) or the initial conditions are localized in space, the amplitude of the resulting mode is proportional to the local value of the adjoint field. Figure 6 can be interpreted as the component of Green's function for the receptivity problem [15].

Finally, we underline that there exists a large difference between the spatial distribution of the direct global mode and the adjoint one, due to the nonnormality of the linearized Navier Stokes operator. The same characteristic is observed in the flow past a circular cylinder [14], and this suggests that neither the use of the direct nor the use of the adjoint field separately can correctly identify the instability mechanism. We therefore perform here a structural sensitivity analysis of the governing operator (for details see, e.g., [14,26]). The resulting structural sensitivity map is depicted in Fig. 7. This map is localized in the region immediately past the sphere. In particular, the maximum of the structural sensitivity field is attained at $x^* = 1.58$, $y^* = 0.48$, $z^* = 0$. We computed this map for several values of the Reynolds number up to $Re = 300$: Results show that the spatial

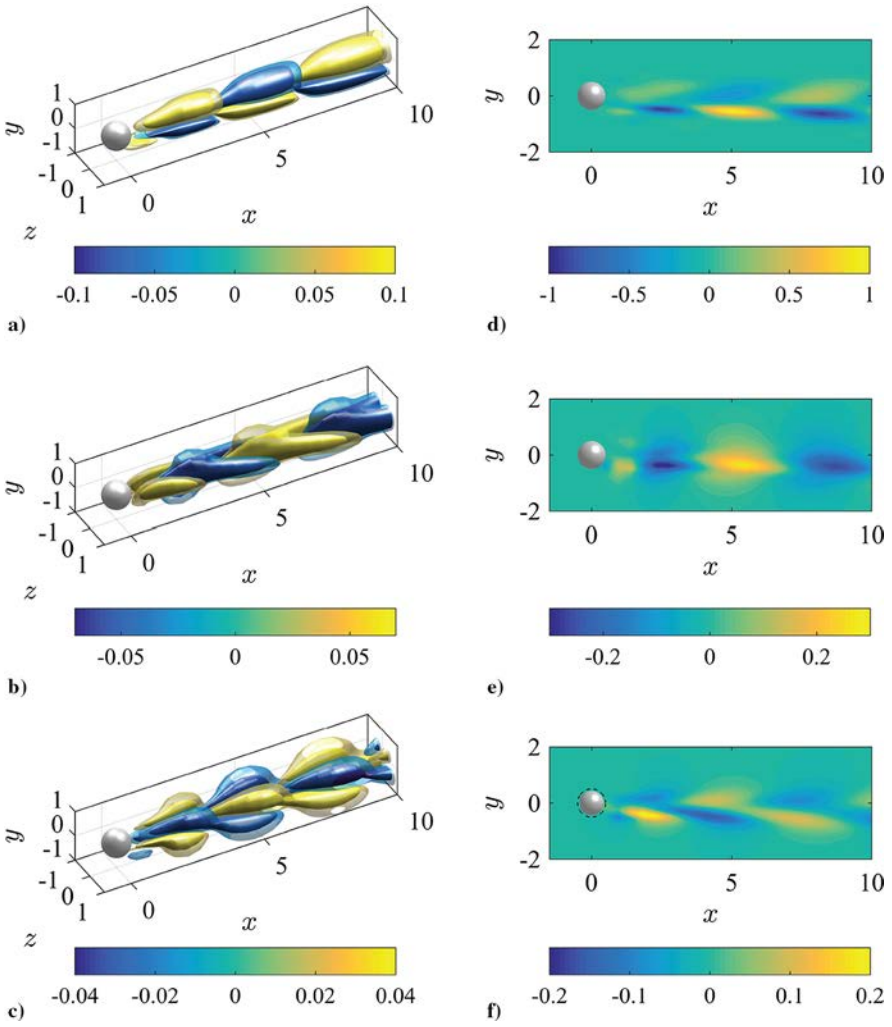

Fig. 5 Unstable direct global eigenmode at $Re = 275$. Depiction of the real part of the complex mode: (left) representative isosurfaces for the velocity components a) $\hat{u}$, b) $\hat{v}$, c) $\hat{w}$; (right) sectional contour plot at d) $z = 0$, e) $z = 0$, f) $z = 0.25$.

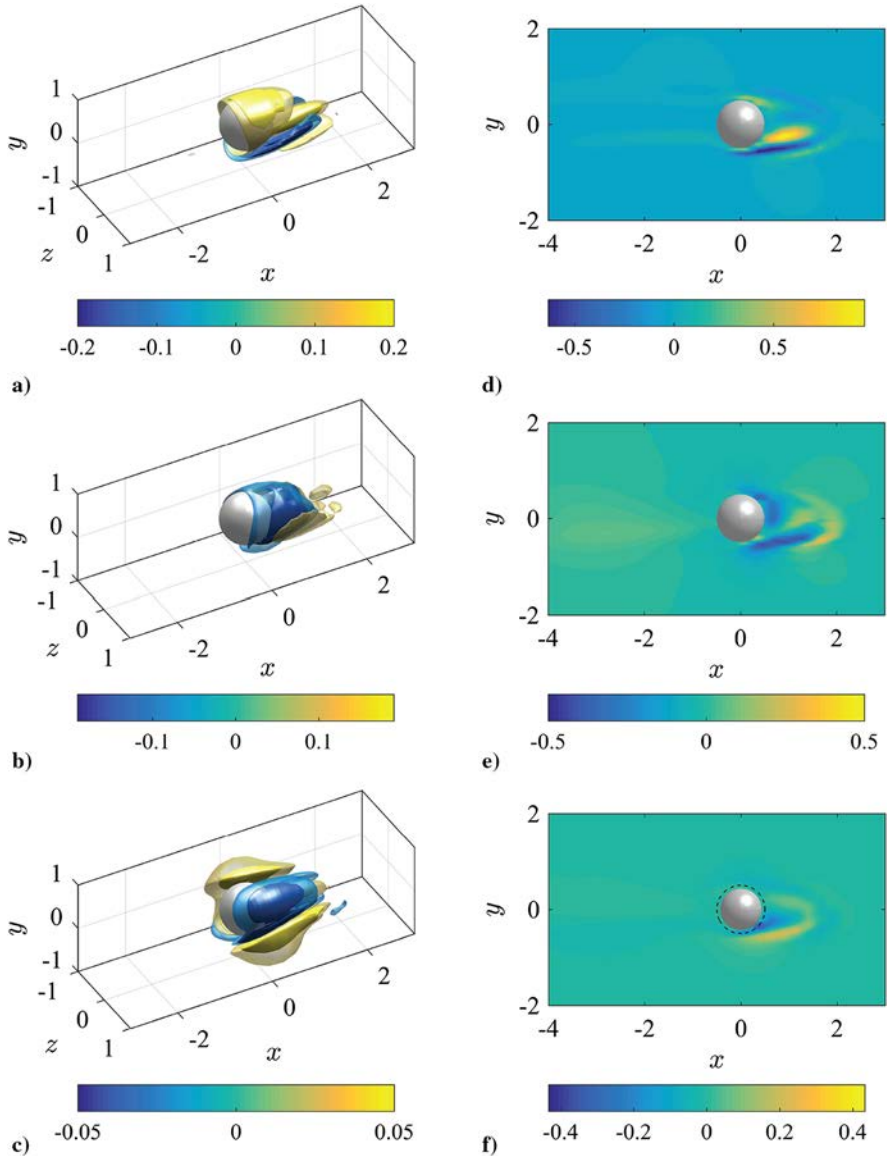

Fig. 6 Leading adjoint global eigenmode at $Re = 275$. Depiction of the real part of the complex mode: (left) representative isosurfaces for the velocity components a) $\hat{u}^{\dagger}$, b) $\hat{v}^{\dagger}$, c) $\hat{w}^{\dagger}$; (right) sectional contour plot at d) $z = 0$, e) $z = 0$, f) $z = 0.25$.

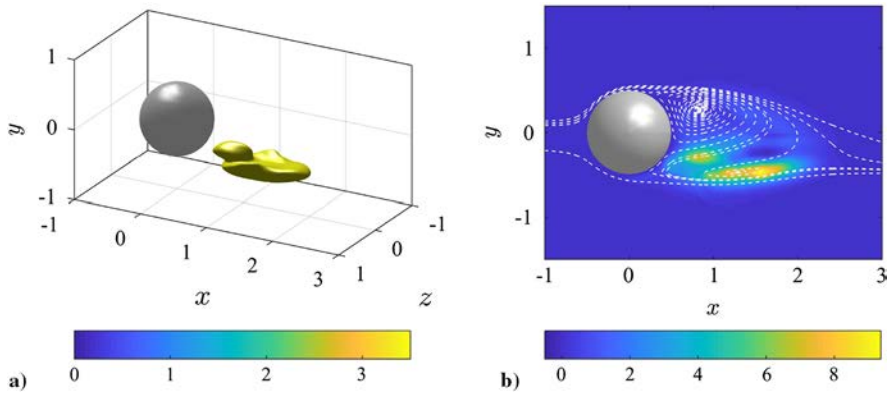

Fig. 7 Structural sensitivity of the leading eigenvalue of the flow past the sphere at $Re = 275$: a) representative isosurfaces of S; b) sectional contour plot at $z = 0$. Gray dashed lines are representative streamlines in the plane at $z = 0$.

structure of the sensitivity is always very similar (not shown here for sake of brevity) to the one reported in Fig. 7. Figure 7b displays the evolution of the streamlines over the bluff body superposed to the isocontours of the sensitivity field. The instability mechanism is driven by the region outside the asymmetric wake: This region is the wavemaker. The other parts of the flow field just respond to the wavemaker excitation, spatially amplifying or dampening the perturbation waves.

Another key point of information is finally provided by the analysis of the sensitivity of the stability characteristics with respect to base

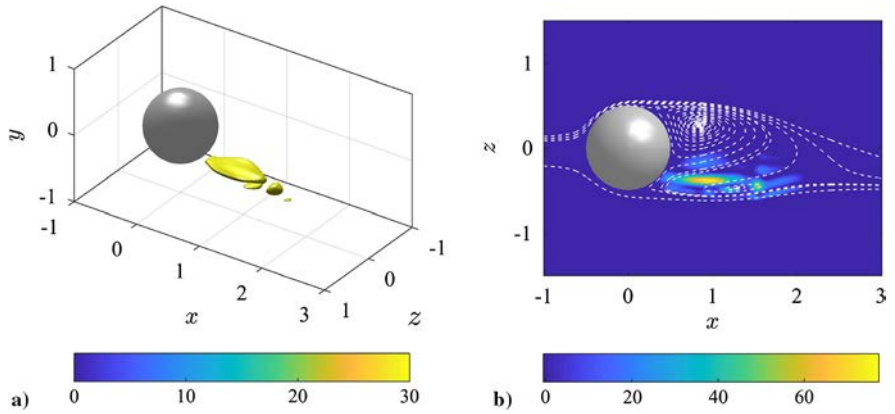

Fig. 8 Sensitivity to base flow modifications of the leading eigenvalue for the flow past a fixed sphere at $Re = 275$. Spatial distribution of the magnitude of the growth rate sensitivity $S_{b,r}$ is shown in terms of a) representative isosurfaces and b) sectional contour plot at $z = 0$. Gray dashed lines are representative streamlines in the plane at $z = 0$.

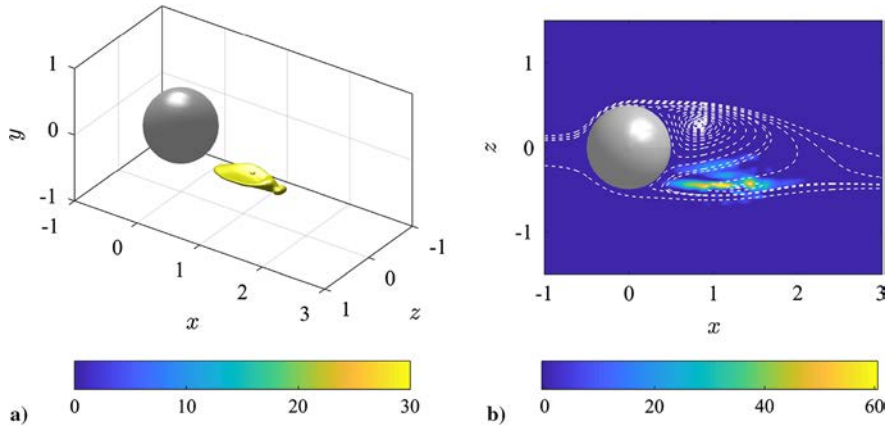

Fig. 9 Sensitivity to base flow modifications of the leading eigenvalue for the flow past a fixed sphere at $Re = 275$. Spatial distribution of the magnitude of the frequency sensitivity $S_{b,i}$ is shown in terms of a) representative isosurfaces and b) sectional contour plot at $z = 0$. Gray dashed lines are representative streamlines in the plane at $z = 0$.

flow changes. In fact, the evolution of perturbations is also affected by modifications at the base flow level. Following the procedure introduced by Marquet et al. [17], we compute the sensitivity to base flow modifications for different Reynolds numbers. The results are depicted in Figs. 8 and 9 for $Re = 275$, where the magnitudes of the growth rate and the frequency sensitivities, respectively, are reported. Both the maps show that the resulting sensitivities reach the highest values in the near wake of the sphere, in regions close to the wavemaker identified by the structural sensitivity map.

V. Conclusions

In the present paper, the stability and sensitivity analysis of the secondary bifurcation occurring in the wake of a sphere has been investigated. Direct numerical simulations show that, increasing the Reynolds number, the flow undergoes a sequence of successive bifurcations. The first pitchfork bifurcation arises at $Re_{\mathrm{cr}}^{\mathrm{I}} = 212.4$, and the inherent flow field is characterized by an asymmetric wake with a single planar symmetry. This paper focuses attention on the secondary instability, which drives the flow to an unsteady state. In particular, the paper's aim is to confirm the existence of a self sustained mode in the asymmetric wake of a fixed sphere. The results discussed in the present work are in agreement with previous numerical and experimental data.

An accurate convergence procedure has been carried out to determine the critical Reynolds number of the second bifurcation $Re_{\mathrm{cr}}^{\mathrm{II}}$. A very weak influence of the grid size and resolution on the leading eigenvalues was found. The resulting critical Reynolds number is 271.8. The spatial distribution of the direct and adjoint eigenmode is analyzed in detail. The direct field is localized downstream from the sphere, and it is characterized by spatial oscillations. The adjoint field, on the other hand, shows that the flow is most receptive to a forcing or to an initial condition localized in the region immediately downstream the bluff body. A structural sensitivity analysis is then performed to identify the core of the instability mechanism. The wavemaker for the second bifurcation is found in the region immediately past the sphere, as for the von Kármán instability of the circular cylinder wake. Finally, the analysis of the sensitivity to a generic base flow modification has been carried out, identifying the regions where the stability properties of the flow are most affected by generic modifications at the base flow level.

References

[1] Taneda, S., "Experimental Investigation of the Wake Behind a Sphere at Low Reynolds Numbers," *Journal of the Physical Society of Japan*, Vol. 11, No. 10, 1956, pp. 1104 1108. doi:10.1143/JPSJ.11.1104

[2] Achenbach, E., "Vortex Shedding from Spheres," *Journal of Fluid Mechanics*, Vol. 62, No. 2, 1974, pp. 209 221. doi:10.1017/S0022112074000644

[3] Sakamoto, H., and Haniu, H., "A Study on Vortex Shedding from Spheres in a Uniform Flow," *Journal of Fluids Engineering*, Vol. 112, No. 4, 1990, pp. 386 392. doi:10.1115/1.2909415

[4] Ormières, D., "Etude Experimentale et Modelisation du Sillage d'une Sphere a bas Nombre de Reynolds," Ph.D. Thesis, Univ. de Provence, Marseille, France, 1999.

[5] Magarvey, R. H., and Bishop, R., "Wakes in Liquid Liquid Systems," *Physics of Fluids*, Vol. 4, No. 7, 1961, pp. 800 805. doi:10.1063/1.1706409

[6] Natarajan, R., and Acrivos, A., "The Instability of the Steady Flow Past Spheres and Disks," *Journal of Fluid Mechanics*, Vol. 254, Sept. 1993, pp. 323 344. doi:10.1017/S0022112093002150

[7] Johnson, T. A., and Patel, V. C., "Flow past a Sphere up to a Reynolds Number of 300," *Journal of Fluid Mechanics*, Vol. 378, Jan. 1999, pp. 19 70. doi:10.1017/S0022112098003206

[8] Tomboulides, A. G., Orszag, S. A., and Karniadakis, G. E., "Direct and Large Eddy Simulation of Axisymmetric Wakes," AIAA Paper 1993 546, 1993.

[9] Ghidersa, B., and Dušek, J., "Breaking of Axisymmetry and Onset of Unsteadiness in the Wake of a Sphere," *Journal of Fluid Mechanics*, Vol. 423, Nov. 2000, pp. 33 69. doi:10.1017/S0022112000001701

[10] Bouchet, G., Mebarek, M., and Dušek, J., "Hydrodynamic Forces Acting on a Rigid Fixed Sphere in Early Transitional Regimes," *European Journal of Mechanics B/Fluids*, Vol. 25, No. 3, 2006, pp. 321 336.

[11] Szaltys, P., Chrust, M., Przadka, A., Goujon Durand, S., Tuckerman, L., and Wesfreid, J., "Nonlinear Evolution of Instabilities Behind Spheres and Disks," *Journal of Fluids and Structures*, Vol. 28, Jan. 2012, pp. 483 487. doi:10.1016/j.jfluidstructs.2011.10.004

[12] Pier, B., "Local and Global Instabilities in the Wake of a Sphere," *Journal of Fluid Mechanics*, Vol. 603, May 2008, pp. 39 61. doi:10.1017/S0022112008000736

[13] Fabre, D., Auguste, F., and Magnaudet, J., "Bifurcations and Symmetry Breaking in the Wake of Axisymmetric Bodies," *Physics of Fluids*, Vol. 20, No. 5, 2008, Paper 051702. doi:10.1063/1.2909609

[14] Giannetti, F., and Luchini, P., "Structural Sensitivity of the First Instability of the Cylinder Wake," *Journal of Fluid Mechanics*, Vol. 581, June 2007, pp. 167 197. doi:10.1017/S0022112007005654

[15] Luchini, P., and Bottaro, A., "Adjoint Equations in Stability Analysis," *Annual Review of Fluid Mechanics*, Vol. 46, No. 1, 2014, pp. 493 517. doi:10.1146/annurev fluid 010313 141253

[16] Bottaro, A., Corbett, P., and Luchini, P., "The Effect of Base Flow Variation on Flow Stability," *Journal of Fluid Mechanics*, Vol. 476, Feb. 2003, pp. 293 302. doi:10.1017/S002211200200318X

[17] Marquet, O., Sipp, D., and Jacquin, L., "Sensitivity Analysis and Passive Control of Cylinder Flow," *Journal of Fluid Mechanics*, Vol. 615, Nov. 2008, pp. 221 252. doi:10.1017/S0022112008003662

[18] Patera, A. T., "A Spectral Element Method for Fluid Dynamics: Laminar Flow in a Channel Expansion," *Journal of Computational Physics*, Vol. 54, No. 3, 1984, pp. 468 488. doi:10.1016/0021 9991(84)90128 1

[19] Fischer, P., "An Overlapping Schwarz Method for Spectral Element Solution of the Incompressible Navier Stokes Equations," *Journal of Computational Physics*, Vol. 133, No. 1, 1997, pp. 84 101. doi:10.1006/jcph.1997.5651

[20] Citro, V., Giannetti, F., Luchini, P., and Auteri, F., "Global Stability and Sensitivity Analysis of Boundary Layer Flows Past a Hemispherical Roughness Element," *Physics of Fluids*, Vol. 27, No. 8, 2015, Paper 084110. doi:10.1063/1.4928533

[21] Tammisola, O., Giannetti, F., Citro, V., and Juniper, M. P., "Second Order Perturbation of Global Modes and Implications for Spanwise Wavy Actuation," *Journal of Fluid Mechanics*, Vol. 755, Sept. 2014, pp. 314 335. doi:10.1017/jfm.2014.415

[22] Lashgari, I., Tammisola, O., Citro, V., Juniper, M. P., and Brandt, L., "The Planar X Junction Flow: Stability Analysis and Control," *Journal of Fluid Mechanics*, Vol. 753, Aug. 2014, pp. 1 28. doi:10.1017/jfm.2014.364

[23] Meliga, P., Chomaz, J. M., and Sipp, D., "Unsteadiness in the Wake of Disks and Spheres: Instability, Receptivity and Control Using Direct and Adjoint Global Stability Analyses," *Journal of Fluids and Structures*, Vol. 25, No. 4, 2009, pp. 601 616. doi:10.1016/j.jfluidstructs.2009.04.004

[24] Fabre, D., Tchoufag, J., Citro, V., Giannetti, F., and Luchini, P., "The Flow Past a Freely Rotating Sphere," *Theoretical and Computational Fluid Dynamics* [online journal], Aug. 2016, pp. 1 0. doi:10.1007/s00162 016 0405 x

[25] Tomboulides, A. G., and Orszag, S. A., "Numerical Investigation of Transitional and Weak Turbulent Flow past a Sphere," *Journal of Fluid Mechanics*, Vol. 416, Aug. 2000, pp. 45 73. doi:10.1017/S0022112000008880

[26] Camarri, S., "Flow Control Design Inspired by Linear Stability Analysis," *Acta Mechanica*, Vol. 226, No. 4, 2015, pp. 979 1010. doi:10.1007/s00707 015 1319 1